Guanidium-assisted crystallization engineering for highly efficient $CsPbI_3$ solar cells

Wang, Shuo ; Xu, Youkui ; Wang, Qian; Zhou, Xufeng ; Li, ZhenHua ; Wang, Meng; Lei, Yutian ; Zhang, Hong ; Wang, Haoxu; Jin, Zhiwen

DOI
10.1039/d2tc01008a

Publication date
2022

Document Version
Final published version

Published in
Journal of Materials Chemistry C

Journal of Materials Chemistry C

ROYAL SOCIETY OF CHEMISTRY

PAPER

View Article Online
View Journal | View Issue

Cite this: J. Mater. Chem. C, 2022, 10, 8234

Guanidium-assisted crystallization engineering for highly efficient $CsPbI_3$ solar cells†

Shuo Wang,[a] Youkui Xu,[a] Qian Wang,*[a] Xufeng Zhou,[b] ZhenHua Li,*[c] Meng Wang,[a] Yutian Lei,[a] Hong Zhang,[d] Haoxu Wang[e] and Zhiwen Jin[a]

Received 12th March 2022,
Accepted 25th April 2022

DOI: 10.1039/d2tc01008a

rsc.li/materials-c

Iodine vacancies and uncoordinated iodide ions of $CsPbI_3$ films are mainly responsible for nonradiative recombination. Here, we report a composition-engineering passivation method that through guanidium (GA^+) and I^- forms strong hydrogen bonds to passivate iodine vacancies and reduce defects. Both experimental and theoretical results confirmed strong chemical interactions between GA^+ and uncoordinated I^- in the $GA_xCs_{1-x}PbI_3$ bulk or at the grain boundary. Moreover, GA^+ doping could slow down the crystallization speed of perovskite films during the deposition process. As a result, we observed GA^+ modified films with much lower defect density, larger grain size, and better carrier extraction and transportation. Upon GA^+ passivation, the power conversion efficiency (PCE) is boosted from 18.01% to 19.05%, with open-circuit voltage (V_{OC}) enhancement from 1.08 V to 1.14 V.

Introduction

Inorganic lead halide perovskites with tunable optoelectronic properties directly derived from their unique structural configuration and chemical versatility have emerged as ranking optoelectronic materials.[1–8] Until now, a power conversion efficiency (PCE) of $CsPbI_3$ perovskite solar cells (PSCs) of over 20% has been achieved.[9–11] Yet, as reported to date, the minimum open-circuit voltage (V_{OC}) loss of inorganic PSCs is 0.45 V, still higher than that of organic–inorganic hybrid PSCs, which is caused by the iodine vacancy and uncoordinated iodide ion induced nonradiative recombination.[12–14] Hence, there is still significant scope for studying how to reduce such nonradiative recombination.[15,16]

To figure out the aforementioned problem, various strategies have been put forward including interface engineering, composition engineering, and solution engineering.[17–19] When it comes to interface engineering, Liu *et al.* employed histamine (HA) as the interface passivation layer on the top of $CsPbI_{3-x}Br_x$.[9] HA, a kind of Lewis base, can coordinate with halide vacancies and undercoordinated lead ions to passivate perovskite surface defects by forming Lewis base–acid.[20,21] However, as reported to date, interface processing may cause a negative work function shift, which activates halide migration to exacerbate device instability.[22–24] Therefore, it is vital to develop a one-step passivation approach.[25]

Guanidium (GA^+), a cation that is analogous to HA, is generally regarded as one of the crucial ions in the formation of alternating cation (ACI) type inorganic–organic two-dimensional perovskites.[26,27] Additionally, previous studies found that GA^+ can improve the crystallization quality of three-dimensional (3D) perovskites and the photovoltaic (PV) performance of the corresponding PSCs.[28] The approximate zero dipole moment and three symmetrical amine groups endow GA^+ with the ability to improve the PV performance of 3D PSCs.[29] On the one hand, GA^+ can form strong hydrogen bonds with adjacent iodide ions, which can inhibit the formation of iodine vacancies and passivate incompatible iodine.[26] On the other hand, GA^+ possesses an approximately zero dipole moment, which has been hypothesized to influence ionic motion appreciably under bias induction.[29] Hence, GA^+ holds great promise in the performance optimization of 3D PSCs.

In this work, a GA^+ optimization strategy was introduced in $CsPbI_3$ PSCs and its influence during perovskite crystallization has also been systematically analyzed.[30] X-Ray diffraction (XRD), photoluminescence (PL) and absorption spectra verified the existence of a GA^+-based perovskite, indicating successful film fabrication. Then, density functional theory (DFT) was

[a] School of Physical Science and Technology & Key Laboratory for Magnetism and Magnetic Materials of the Ministry of Education, Lanzhou University, Lanzhou 730000, China. E-mail: qianwang@lzu.edu.cn
[b] School of Material Science and Engineering, Liaocheng University, Liaocheng 252000, China
[c] School of Physical Science and Technology & Lanzhou Center for Theoretical Physics & Key Laboratory of Theoretical Physics of Gansu Province, Lanzhou University, Lanzhou 730000, China. E-mail: lizhenhua@lzu.edu.cn
[d] Electron Microscopy Centre of Lanzhou University, School of Materials and Energy, Lanzhou University, Lanzhou 730000, China
[e] Delft University of Technology, Photovoltaic Materials and Devices Group, Mekelweg 4, 2628 CD Delft, The Netherlands

† Electronic supplementary information (ESI) available: Synthesis details and additional figures. See DOI: https://doi.org/10.1039/d2tc01008a

employed to explore the role of GA^+ during crystal crystallization, and the results reveal that the $CsPbI_3$ structure remains 3D and the average length of Pb–I bonds would be longer, reducing the overlap of the Pb s-orbitals and I p-orbitals.[31–33] Meanwhile, the formation of grain boundaries and defects was apparently restrained owing to the optimization effect of GA^+ on crystallization kinetics. Consequently, GA^+ doped PSCs exhibit a larger grain size and smoother morphology, which is beneficial for V_{OC} increase and defect-driven nonradiative recombination inhibition.[34,35] As a result, the champion PSC achieved a stabilized PCE of 19.05% and a V_{OC} of 1.14 V.

Results and discussion

To study the role of GA^+ in the PV performance of PSCs, perovskites with a composition of $GA_xCs_{1-x}PbI_3$ (x = 0%, 1%, 3% and 5%) were deposited on a fluorinated tin dioxide (FTO)/titanium dioxide (TiO_2) substrate. The detailed structures of the optimized $CsPbI_3$ film and the GA^+ molecule are shown in Fig. 1(a).[36,37] The specific structure of PSCs is shown in Fig. S1a (ESI†). Fig. S1b (ESI†) depicts cross-section SEM images, revealing dense, compact, and uniform $GA_xCs_{1-x}PbI_3$ films with a thickness of 500 nm. Then XRD was employed to investigate the changes in the crystallographic structures.

As illustrated in Fig. 1(b), all kinds of films show two characteristic peaks of $GA_xCs_{1-x}PbI_3$ positioned at 14.1° and 28.2°, corresponding to the (100) and (200) lattice planes, respectively.[38] With increasing GA^+, these two characteristic peaks shift to larger angles, indicating lattice shrinking induced by hydrogen bonds formed by GA^+ and halide ions. Generally, the lattice size was determined by the synergistic effect of the contractile force from strong hydrogen bonds and the expansion force from GA^+. Thus, the lattice size and GA^+ concentration did not conform to a linear relationship.[39] Chemical compositions of the resultant films were studied by X-ray photoelectron spectroscopy (XPS), and the spectrum of nitrogen is shown in Fig. 1(c). We can observe that the peak of N 1S appears only in films (3%), which indicates that GA^+ was incorporated into $CsPbI_3$ successfully, and is also exhibited in XRD results. Additionally, the spectra of I 3d, Cs 3d, and Pb 4f are shown in Fig. S2 (ESI†).[40]

Then scanning electron microscopy (SEM) was adopted to further explore the effect of GA^+ impact on $CsPbI_3$ film morphology. The SEM images are shown in Fig. 2(a)–(d), and it is distinct that all perovskite films have grown with full coverage on the substrate. Compared with the reference film (0%) (Fig. 2(a)), Fig. 2(b)–(d) show GA^+-treated films at different concentrations (1%, 3%, and 5%) revealing a larger average grain size, which also could be extracted intuitively from the statistical chart of grain size (Fig. 2(e)–(h)). With the increase of GA^+, the size of most grains becomes larger. When it comes to the average grain size, the film (3%) (Fig. 2(g)) has the largest average grain size with fewer grain boundaries, which is the result of control of the crystallization kinetics by GA^+ doping.[41] Moreover, it could be observed that film (3%) morphology is more uniform and denser with fewer grain boundaries, suggesting a lower defect density, which could reduce defect-driven nonradiative recombination.[42,43]

To further investigate the roughness of the resulted films, atomic force microscopy (AFM) was deployed to measure the surface roughness of the film (0%) and the film (3%).[44] As shown in Fig. 2(i) and (j), film (3%) showed a lower reduction in

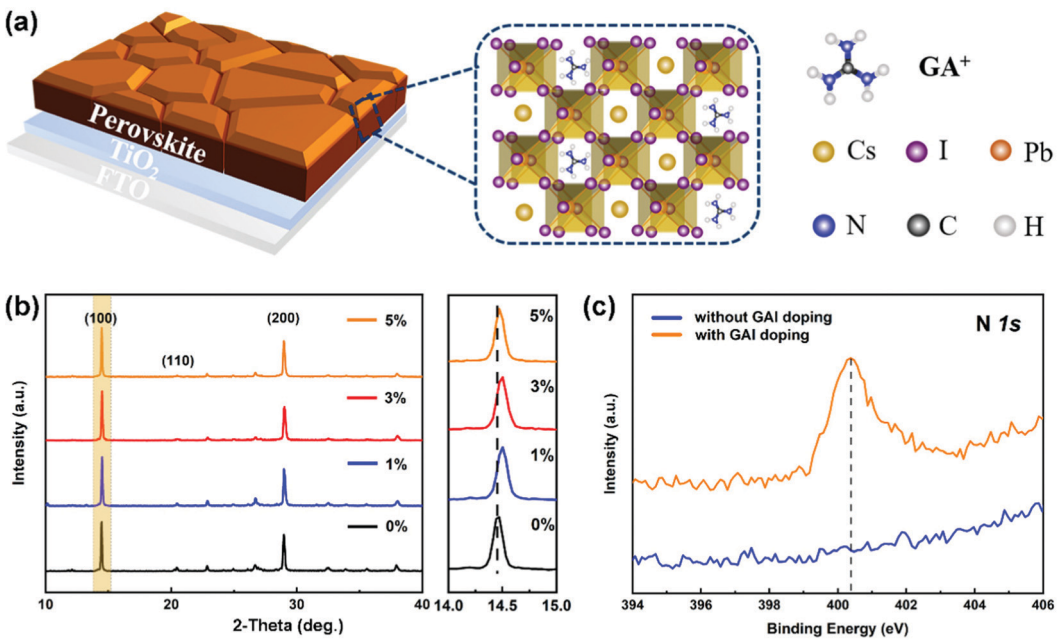

Fig. 1 Composition characterization of the $CsPbI_3$ films: (a) schematic view of the depth-dependent manipulation strategy, (b) XRD patterns and (c) surface XPS spectrum of N 1s.

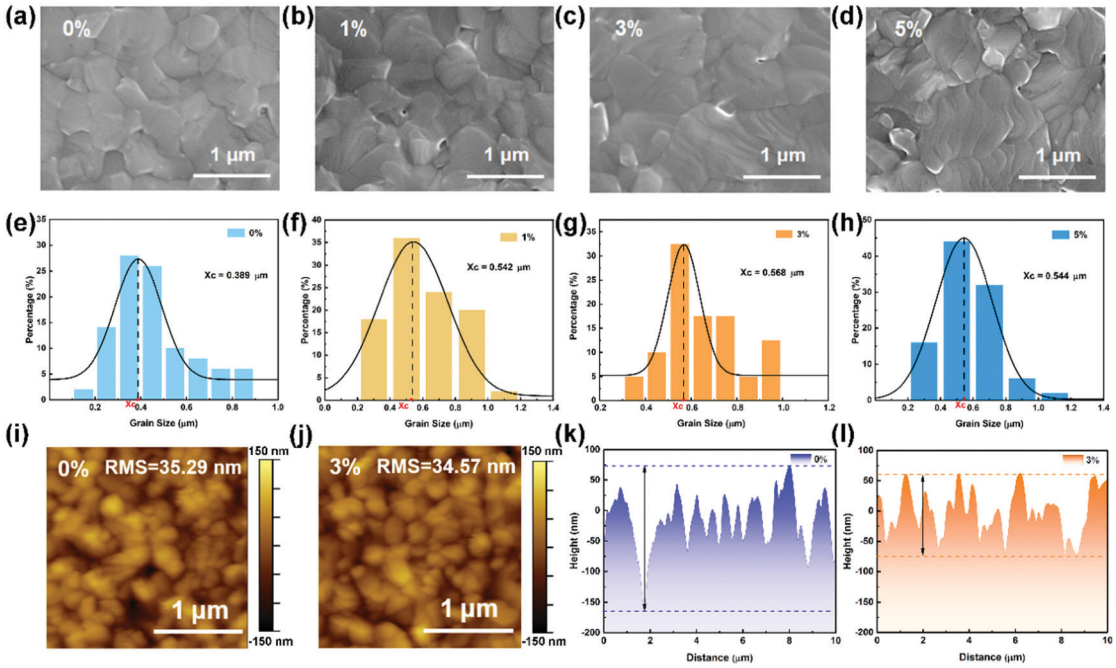

Fig. 2 Surface morphology characterization of the $CsPbI_3$ films with different GA^+ doping: (a)–(d) top-view SEM images; (e)–(h) statistics of grain sizes; (i) and (j) AFM images and (k), (l) cross-sectional height images.

the surface roughness of 34.57 nm in contrast to 35.29 nm of the film (0%). In addition, the flatness of the film was extracted from Fig. 2(k) and (l). In comparison to the film (0%), the film (3%) exhibited a smoother section and better film continuity.

Then, DFT calculations were employed to reveal the underlying mechanism about the relationship between GA^+ substitution and crystal structures, assuming a X ($GA_xCs_{1-x}PbI_3$) value of 12.5% in this process.[45] Initially, we anticipated a negligible crystal structure change after GA^+ substitution, as is shown in Fig. 3(a). Surprisingly, the calculated results revealing an obvious lattice distortion (Fig. 3(b)) and then resulting in a volume contraction (from 2111.08 $Å^3$ to 1994.49 $Å^3$), which is consistent with the results of XRD patterns. The interlayer structure of $GA_xCs_{1-x}PbI_3$ is shown in Fig. 3(c). The bandgap value was extracted from Fig. 3(d) and (e). Compared to pure $CsPbI_3$, the bandgap of $GA_xCs_{1-x}PbI_3$ shows obvious enlargement. It was increased from 1.37 eV to 1.55 eV.[46] The increase of the perovskite average bandgap is closely relevant to the changes of the lattice internal structure.[47] The result was also reflected in the PL spectra (Fig. S3a, ESI†) and absorption

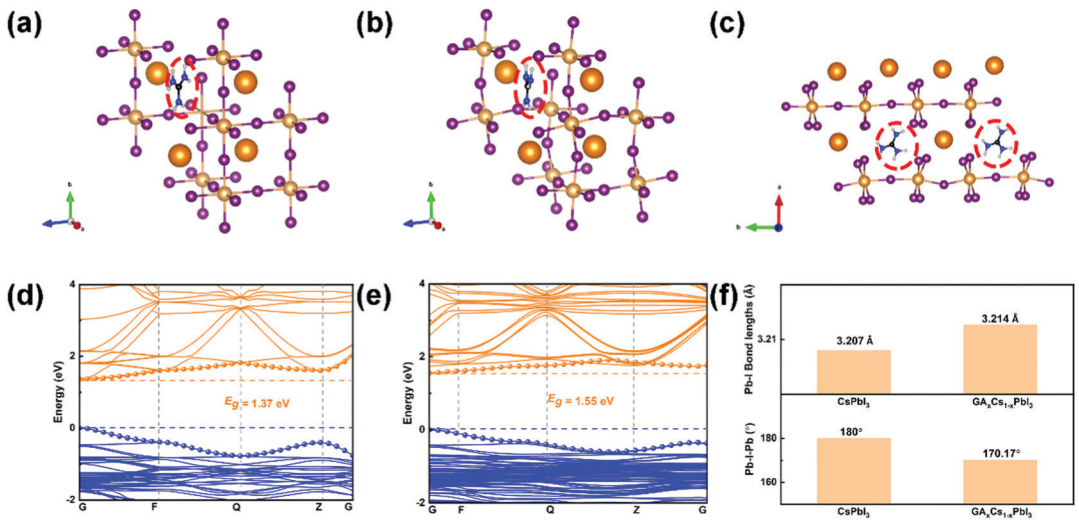

Fig. 3 Structural characterization and DFT calculations of $GA_xCs_{1-x}PbI_3$ structures: (a) ideal doping simulation, (b), (c) practical doping simulation, (d), (e) DFT calculations of band structures of $CsPbI_3$ film with and w/o GAI doping, respectively; (f) average Pb–I bond length and average Pb–I–Pb angle of $CsPbI_3$ film with and w/o GAI doping.

spectra (Fig. S3b, ESI†). As shown in Fig. 3f, average statistics by measurement showed that the lengths of Pb–I bonds increase from 3.207 Å to 3.214 Å. The average Pb–I–Pb angles were 180° and 170.17° for pure $CsPbI_3$ and $GA_xCs_{1-x}PbI_3$, respectively. The enlargement of the bandgap was attributed to the elongation of the Pb–I bond, which can decrease the overlap of Pb s-orbitals and I p-orbitals, thereby resulting in an enlarged bandgap.[48,49]

The typical *J–V* curves and other PV parameters are shown in Fig. 4(a) and Table S1 (ESI†). As can be seen in Fig. 4(a) and Table 1, the V_{OC} and PCE of the 3% device was 1.14 V and 19.05%, and that of the reference device was 1.08 V and 18.01%. When the concentration of GAI increased to 5%, the PCE would decrease to 16.88% despite a higher V_{OC} in comparison to the original one, which was owing to the rather low fill factor (FF) which was triggered by the inferior quality of the $GA_xCs_{1-x}PbI_3$ film.[50] To study reproducibility and regularity more intuitively, ten individual devices were prepared based on different perovskites as shown in Fig. 4(b), which lists the PV parameters of the reference devices (0%) and the optimal one (3%). We can extracted from it that V_{OC} and PCE have a markable improvement as well. Simultaneously, short-circuit current density (J_{SC}) and FF of 3% are pretty much the same as 0%.

In terms of *J–V* curves, the forward and reverse scanning data of the reference device and the champion device can be seen in Fig. S4a, b and Tables S1, S2 (ESI†). We can conclude that the hysteresis phenomenon was manifested more obviously in GA-modified devices. About this appearance, previous studies have found that increased capacitance caused by the accumulation of excess GA^+ in GA-treated PSCs increases the capacitance in the low-frequency region, resulting in current hysteresis. In addition, the applied bias-induced ionic motion amplified the hysteresis by shielding the internal electric field at the interface between the TiO_2 layer and the $GA_xCs_{1-x}PbI_3$ layers.[51]

Fig. 4(c) schematically illustrates the corresponding external quantum efficiency (EQE) spectra and integrated J_{SC} of the reference device (0%) and the optimal one (3%). The integrated J_{SC} matched well with the practical measurement value with about 5% deviation. The EQE spectra responded in a wide range wavelength from 300 nm to 800 nm. In contrast to the 0% device, the 3% one showed barely any change, which matched well with the characterization of J_{SC} as shown in Fig. S4b (ESI†).

Table 1 The photovoltaic parameters of the reference $CsPbI_3$ PSCs w/wo GA^+ doping under reverse scan directions (extracted from Fig. 4(a))

Device (%)	J_{SC} (mA cm^{-2})	V_{OC} (V)	FF (%)	PCE (%)
0	20.70	1.08	80.30	18.01
1	20.73	1.11	79.51	18.36
3	20.70	1.14	80.70	19.05
5	20.80	1.04	77.75	16.88

The plots of PCE and J_{SC} as a function of time are shown in Fig. 4(d). The PCE of the resulting devices based on the film (0%) and the film (3%) stabilized at 17.9% and 19.0%, with J_{SC} of 20.3 mA cm^{-2} and 20.6 mA cm^{-2}, respectively, which matched the values obtained from the *J–V* curves well.[52] In addition, all PV parameters of the resulting devices were also recorded. As can be deduced from Fig. S3c (ESI†), all devices show a linear relationship of J_{SC} *versus* light intensity, indicating negligible bimolecular recombination; results can be expressed as $J_{SC} \propto I^{\alpha}$.[53] In contrast to the reference device (0%), the more ideal α value (1.026) suggests a reduced trap density within the films (3%). Fig. 4(e) showed the relationship of V_{OC} *versus* light intensity. According to this equation, the slope is derived from a straight line that fits linearly to the data: $V_{OC} \propto nkT/q \ln(I)$.[54] As can be seen that the device with film (3%) has smaller slope at 1.53 kT/q. Given to the previous reports, the deviation of value of slope from 1 kT/q manifests trap-assisted recombination, which is one of main causes for V_{OC} loss. Hence, a smaller slope indicates a more significant suppression of trap-assisted recombination, which could lead to obvious enhancement of V_{OC}.

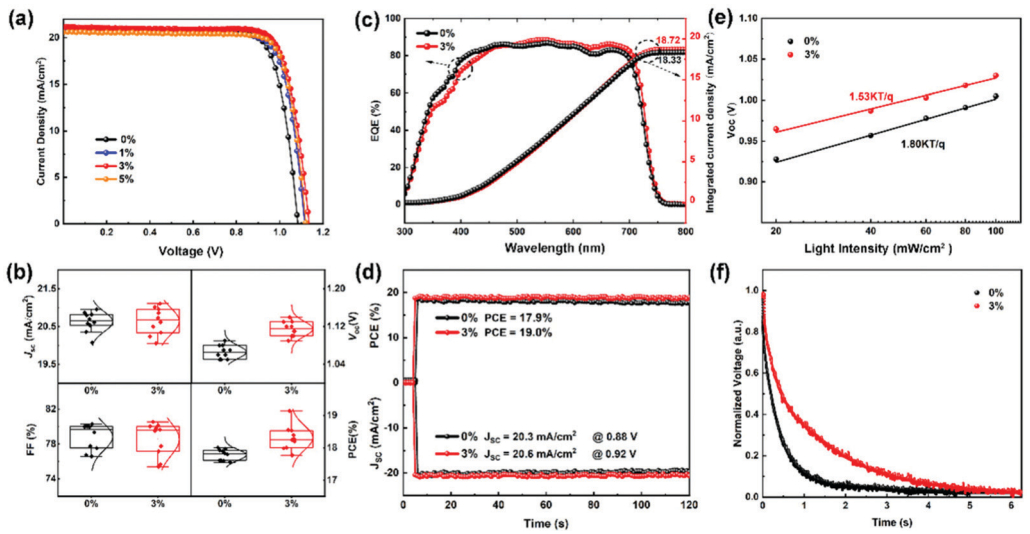

Fig. 4 Photovoltaic performance characterization of the $CsPbI_3$ PSCs with different GA^+ doping: (a) *J–V* curves; (b) statistical J_{SC}, V_{OC}, FF and PCE for fifteen independent devices; (c) EQE spectra; (d) *I–T* curves; (e) light intensity dependence for V_{OC} and (f) stable-state photovoltage attenuation curves.

The charge-transport properties of the GA^+ optimized PSCs were investigated by the stable-state photocurrent decay (Fig. S3d, ESI†) and the stable-state photovoltage decay (Fig. 4(f)) measurements. The semblable response of stable-state photocurrent decay suggested that the doping of GA^+ had minimal influence on the charge-transport properties or charge-collection efficiency, which is in accordance with J_{SC} of box-plots (Fig. 4(b)) and EQE (Fig. 4(c)).[55] In contrast, the photovoltage revealed that GA^+-treatment enhanced the charge-carrier lifetime, which also indicated that GA^+ decreased the undesired charge-carrier recombination. This further proved that GA^+ could inhibit the existence of halide vacancies and passivate incompatible halide species by strong hydrogen bonds capability, leading to the significant enhancement of charge-carrier lifetime.

The aforementioned result could also be extracted from Fig. S3e (ESI†), which presents the time-resolved PL (TRPL) spectra of $GA_xCs_{1-x}PbI_3$ films fabricated on FTO/TiO_2 substrates. The corresponding curves were fitted by biexponential decay function [Time (τ_i) and amplitudes (A_i)].[56] The average carrier lifetime (τ_{ave}) was calculated by $\tau_{ave} = \Sigma A_i\tau_i^2/\Sigma A_i\tau_i$.[35] It can be obtained that the film (3%) has a much shorter τ_{ave} of 3.853 ns than the film (0%) (7.189 ns). The significantly shortened charge-carrier lifetime is mainly attributed to better carrier extraction of the TiO_2 layer, which is in accordance with the results of stable-state photocurrent decay (Fig. S3d, ESI†).

In addition, the dark current could be used to characterize the trap density (N_t), which could be computed by applying space charge-limited current (SCLC) measurements. The dark current curves of electron-only devices are shown in Fig. 5(a) and (b). It can be found that the film (3%) has smaller trap-filled limit voltage (V_{TFL}) (0.154 V) in contrast to the film (0%) (0.179 V), which is attributed to a better morphology and GA^+ passivating effect. The relationship of V_{TFL} and N_t is according to $N_t = 2V_{TFL}\varepsilon_r\varepsilon_0/eL^2$,[57] where ε_r is the relative dielectric constant of $GA_xCs_{1-x}PbI_3$, ε_0 is the vacuum permittivity, L is the thickness of the $GA_xCs_{1-x}PbI_3$ films (Fig. S1b, ESI†), and e is the elementary electric charge. The calculated trap density of electron-only devices based on the films (0%) and the films (3%) are about 6.5×10^{14} cm^{-3} and 5.8×10^{14} cm^{-3}, respectively. In addition, the electron mobility could be estimated by the equation of $\mu = 8J_DL^3/9\varepsilon_r\varepsilon_0V_{bi}^2$,[58] where J_D is the current density. The electron mobility of devices based on the films (0%) and the films (3%) are 8.08×10^{-3} cm^{-2} V^{-1} s^{-1} and 1.43×10^{-2} cm^{-2} V^{-1} s^{-1}, respectively, which is in accordance with the reduction of the carrier lifetime as observed in Fig. S3e (ESI†). Similarly, as shown in Fig. 5(c) and (d), we obtained the trap density of hole-only devices based on the films (0%) and the films (3%) to be about 1.2×10^{15} cm^{-3} and 9.5×10^{15} cm^{-3}, respectively. And the hole mobility of devices based on the films (0%) and the films (3%) are 1.61×10^{-4} cm^{-2} V^{-1} s^{-1} and 1.43×10^{-4} cm^{-2} V^{-1} s^{-1}, respectively, which further suggested that charge carrier transportation could be enhanced after GA^+ doping.

To probe contact resistance information at the interface of $GA_xCs_{1-x}PbI_3$ layer, we performed electrical impedance spectroscopy (EIS) as can be observed in Fig. 5(e). The equivalent circuit models can be observed in Fig. 5(e) insert, including recombination capacitance (C_{rec}), series resistance (R_s), and shunt resistance (R_{sh}). The Nyquist plots showed that the devices with different films exhibit distinct semicircles at low frequencies.[59] Previous studies found that the low-frequency region represents the recombination process. Hence, a larger semicircle of devices based on the film (3%) suggested efficient suppression of recombination by GA^+ doping, which is due to strong hydrogen bonds formed by GA^+ and halide ions. Fig. 5(f)

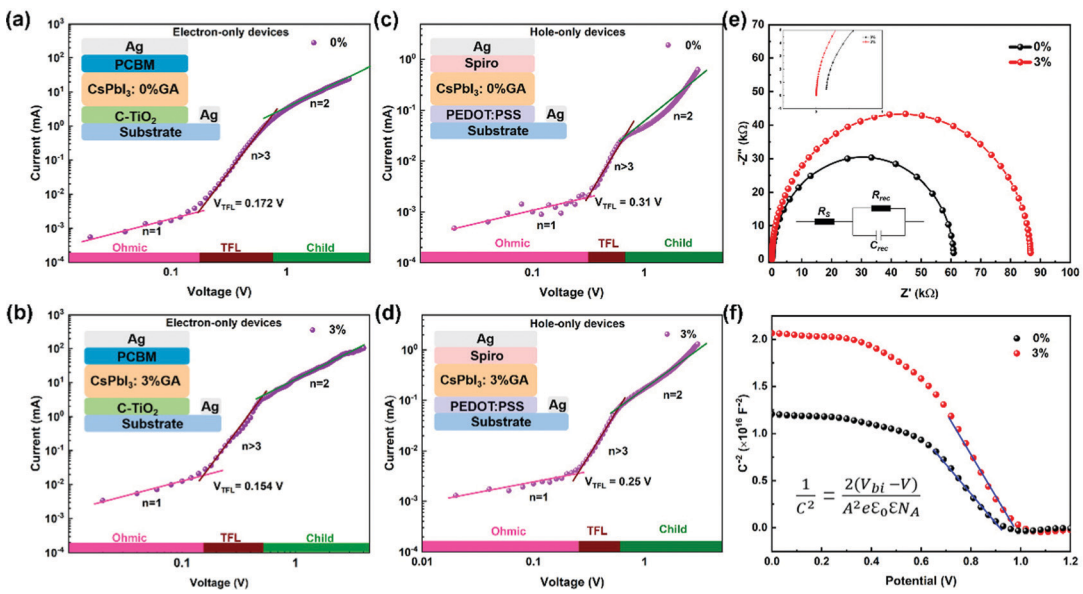

Fig. 5 Defect characterization of the $CsPbI_3$ PSCs: the dark J–V measurements of (a) and (b) electron-only devices and (c), (d) hole-only devices; (e) electrical impedance spectroscopy (EIS) data; and (f) capacitance–voltage curves.

showed the Mott–Schottky (M–S) plots of reference devices (0%) and GA^+-treated devices (3%).

The relationship of build-in potential (V_{bi}) and donor density (N_A) can be calculated by the following function:[60]

$$\frac{1}{C^2} = \frac{2(V_{bi} - V)}{A^2 e \varepsilon_0 \varepsilon N_A}$$

where C, V, A, ε_0, ε and e denote the depletion layer capacitance, applied voltage, electrode area, permittivity of vacuum, dielectric constant of the sample and electronic charge. As can be observed, the V_{bi} value of the reference device (0%) is 0.95 V, lower than the 3% one (1.03 V), which means that the device (3%) can extract photogenerated carrier more efficiently. Fig. S4c (ESI†) displays the stability of result devices, normalized PCE changes of devices based on the films (0%) and the films (3%) at different storage times showed that both devices can keep over 98% of the original value, which can prove that GA^+ doping would not reduce the stability of $CsPbI_3$.

Conclusions

In conclusion, we proved that GA^+ doping is an effective approach to enhance the PV performance of PSCs. The synergistic effect of GA^+ and I^- was observed. Hence, the optimized films showed superior carrier transportation and extraction ability. Remarkably, optimized PSCs showed reduced loss of V_{OC} and boosted PCE. The optimal device was obtained for $CsPbI_3$ with 3% GA^+, with a champion PCE of 19.05% and a V_{OC} of 1.14 V. In the meantime, the GA^+-incorporated device showed great stability which can maintain 98% of its initial efficiency after 240 h when stored in the nitrogen atmosphere glove box.

Author contribution statement

S. W., Y. L., M. W., and Y. X. performed the experiments, data analysis, and experimental planning. The project was conceived, planned and supervised by S. W., Y. X., Y. L., and M. W. Some of the experimental tests were supported by Z. L., X. Z., and H. Z. The manuscript was written by S. W., Q. W., H. W., and Z. J. All the authors reviewed the manuscript.

Conflicts of interest

The authors declare no competing financial interests.

Acknowledgements

This work was funded by the National Natural Science Foundation of China (52073131 and 51902148), the Fundamental Research Funds for the Central Universities (lzujbky-2021-it31, lzujbky-2021-59, lzujbky-2021-ct15, lzujbky-2021-ct01 and lzujbky-2021-sp69), and National Natural Science Foundation of China (12047501), and the calculation work was supported by the Supercomputing Center of Lanzhou University.

References

1 M. A. Green, A. Ho-Baillie and H. J. Snaith, *Nat. Photonics*, 2014, **8**, 506–514.
2 J. Burschka, N. Pellet, S. J. Moon, R. Humphry-Baker, P. Gao, M. K. Nazeeruddin and M. Gratzel, *Nature*, 2013, **499**, 316–319.
3 N. J. Jeon, J. H. Noh, W. S. Yang, Y. C. Kim, S. Ryu, J. Seo and S. I. Seok, *Nature*, 2015, **517**, 476–480.
4 T. Zhang, M. I. Dar, G. Li, F. Xu, N. Guo, M. Grätzel and Y. Zhao, *Sci. Adv.*, 2017, **3**, e1700841.
5 J. Duan, J. Wei, Q. Tang and Q. Li, *Sol. Energy*, 2020, **195**, 644–650.
6 Z. Yang, Z. Yu, H. Wei, X. Xiao, Z. Ni, B. Chen, Y. Deng, S. N. Habisreutinger, X. Chen, K. Wang, J. Zhao, P. N. Rudd, J. J. Berry, M. C. Beard and J. Huang, *Nat. Commun.*, 2019, **10**, 4498.
7 Z. Li, F. Zhou, H. Yao, Z. Ci, Z. Yang and Z. Jin, *Mater. Today*, 2021, **48**, 155–175.
8 Y. Miao, L. Cheng, W. Zou, L. Gu, J. Zhang, Q. Guo, Q. Peng, M. Xu, Y. He, S. Zhang, Y. Cao, R. Li, N. Wang, W. Huang and J. Wang, *Light: Sci. Appl.*, 2020, **9**(1), 89.
9 X. Gu, W. Xiang, Q. Tian and S. Liu, *Angew. Chem., Int. Ed.*, 2021, **60**, 23164–23170.
10 H. Yao, S. Shi, Z. Li, Z. Ci, G. Zhu, L. Ding and Z. Jin, *J. Energy Chem.*, 2021, **57**, 567–586.
11 W. Sharmoukh, S. A. Al Kiey, B. A. Ali, L. Menon and N. K. Allam, *Sustainable Mater. Technol.*, 2020, **26**, e00210.
12 J. Yuan, X. Ling, D. Yang, F. Li, S. Zhou, J. Shi, Y. Qian, J. Hu, Y. Sun, Y. Yang, X. Gao, S. Duhm, Q. Zhang and W. Ma, *Joule*, 2018, **2**, 2450–2463.
13 L. Zhang, T. Jia, L. Pan, B. Wu, Z. Wang, K. Gao, F. Liu, C. Duan, F. Huang and Y. Cao, *Sci. China: Chem.*, 2021, **64**, 408–412.
14 Y. Lei, Y. Xu, M. Wang, G. Zhu and Z. Jin, *Small Methods*, 2021, **17**, 2005495.
15 W.-Q. Wu, P. N. Rudd, Z. Ni, C. H. Van Brackle, H. Wei, Q. Wang, B. R. Ecker, Y. Gao and J. Huang, *J. Am. Chem. Soc.*, 2020, **142**, 3989–3996.
16 C. Chen, X. Wang, Z. Li, X. Du, Z. Shao, X. Sun, D. Liu, C. Gao, L. Hao, Q. Zhao, B. Zhang, G. Cui and S. Pang, *Angew. Chem., Int. Ed.*, 2021, **61**, e202113932.
17 Y. He, Z. Tang, L. Mao, S. Yang, T. Yang, M. Xie, Q. Chang, L. Ding, B. He, C. Peng, C. Yu, X. Hao, J. Zhang, K. Zheng, C. Han, Y. Zhang, H. Yan and X. Xu, *Phys. Status Solidi RRL*, 2021, **15**, 2100119.
18 S. Yang, J. Dai, Z. Yu, Y. Shao, Y. Zhou, X. Xiao, X. C. Zeng and J. Huang, *J. Am. Chem. Soc.*, 2020, **142**, 11937–11938.
19 Y. Guo, H. Liu, W. Li, L. Zhu and H. Chen, *Sol. RRL*, 2020, **4**, 2000380.
20 T. Wu, Y. Wang, X. Li, Y. Wu, X. Meng, D. Cui, X. Yang and L. Han, *Adv. Energy Mater.*, 2019, **9**, 1803766.
21 C. Chen, J. Hu, Z. Xu, Z. Wang, Y. Wang, L. Zeng, X. Liu, Y. Li, Y. Mai and F. Guo, *Adv. Compos. Hybrid Mater.*, 2021, **4**, 1261–1269.
22 S. Tan, T. Huang, I. Yavuz, R. Wang, T. W. Yoon, M. Xu, Q. Xing, K. Park, D.-K. Lee, C.-H. Chen, R. Zheng, T. Yoon,

Y. Zhao, H.-C. Wang, D. Meng, J. Xue, Y. J. Song, X. Pan, N.-G. Park, J.-W. Lee and Y. Yang, *Nature*, 2022, DOI: 10.1038/s41586-022-04604-5.
23 W. Zhu, Q. Wang, W. Chai, D. Chen, D. Chen, J. Chang, J. Zhang, C. Zhang and Y. Hao, *Org. Electron.*, 2020, **78**, 105598.
24 J. Chen and N.-G. Park, *Adv. Mater.*, 2019, **31**, 1803019.
25 M. Wang, Z. Zang, B. Yang, X. Hu, K. Sun and L. Sun, *Sol. Energy Mater. Sol. Cells*, 2018, **185**, 117–123.
26 Y. Zhou, H. Xue, Y.-H. Jia, G. Brocks, S. Tao and N. Zhao, *Adv. Funct. Mater.*, 2019, **29**, 1905739.
27 Y. Xu, M. Wang, Y. Lei, Z. Ci and Z. Jin, *Adv. Energy Mater.*, 2020, **10**, 2002558.
28 Y. Zheng, X. Yang, R. Su, P. Wu, Q. Gong and R. Zhu, *Adv. Funct. Mater.*, 2020, **30**, 2000457.
29 N. De Marco, H. Zhou, Q. Chen, P. Sun, Z. Liu, L. Meng, E.-P. Yao, Y. Liu, A. Schiffer and Y. Yang, *Nano Lett.*, 2016, **16**, 1009–1016.
30 H. Wang, Z. Dong, H. Liu, W. Li, L. Zhu and H. Chen, *Adv. Energy Mater.*, 2021, **11**, 2002940.
31 D. M. Trots and S. V. Myagkota, *J. Phys. Chem. Solids*, 2008, **69**, 2520–2526.
32 X. Li, Y. Fu, L. Pedesseau, P. Guo, S. Cuthriell, I. Hadar, J. Even, C. Katan, C. C. Stoumpos, R. D. Schaller, E. Harel and M. G. Kanatzidis, *J. Am. Chem. Soc.*, 2020, **142**, 11486–11496.
33 H. J. Kim, A. Konarov, J. H. Jo, J. U. Choi, K. Ihm, H.-K. Lee, J. Kim and S.-T. Myung, *Adv. Energy Mater.*, 2019, **9**, 1901181.
34 L. Zhang, X. Yang, Q. Jiang, P. Wang, Z. Yin, X. Zhang, H. Tan, Y. Yang, M. Wei, B. R. Sutherland, E. H. Sargent and J. You, *Nat. Commun.*, 2017, **8**, 15640.
35 M. Stolterfoht, C. M. Wolff, J. A. Márquez, S. Zhang, C. J. Hages, D. Rothhardt, S. Albrecht, P. L. Burn, P. Meredith, T. Unold and D. Neher, *Nat. Energy*, 2018, **3**, 847–854.
36 E. Jokar, C.-H. Chien, C.-M. Tsai, A. Fathi and E. W.-G. Diau, *Adv. Mater.*, 2019, **31**, 1804835.
37 Y. Zhang, Y. Wang, L. Zhao, X. Yang, C.-H. Hou, J. Wu, R. Su, S. Jia, J.-J. Shyue, D. Luo, P. Chen, M. Yu, Q. Li, L. Li, Q. Gong and R. Zhu, *Energy Environ. Sci.*, 2021, **14**, 6526–6535.
38 G. E. Eperon, G. M. Paternò, R. J. Sutton, A. Zampetti, A. A. Haghighirad, F. Cacialli and H. J. Snaith, *J. Mater. Chem. A*, 2015, **3**, 19688–19695.
39 B. Liu, H. Bi, D. He, L. Bai, W. Wang, H. Yuan, Q. Song, P. Su, Z. Zang, T. Zhou and J. Chen, *ACS Energy Lett.*, 2021, **6**, 2526–2538.
40 W. Zhang, J. Xiong, J. Li and W. A. Daoud, *Sol. RRL*, 2020, **4**, 2000112.
41 Y. Ding, Y. Wu, Y. Tian, Y. Xu, M. Hou, B. Zhou, J. Luo, G. Hou, Y. Zhao and X. Zhang, *J. Energy Chem.*, 2021, **58**, 48–54.
42 P. You, G. Tang, J. Cao, D. Shen, T.-W. Ng, Z. Hawash, N. Wang, C.-K. Liu, W. Lu, Q. Tai, Y. Qi, C.-s Lee and F. Yan, *Light: Sci. Appl.*, 2021, **10**(1), 68.
43 K. Yao, S. Li, Z. Liu, Y. Ying, P. Dvorak, L. Fei, T. Sikola, H. Huang, P. Nordlander, A. K.-Y. Jen and D. Lei, *Light: Sci. Appl.*, 2021, **11**(1), 18.
44 A. E. Shalan, W. Sharmoukh, A. N. Elshazly, M. M. Elnagar, S. A. Al Kiey, M. M. Rashad and N. K. Allam, *Sustainable Mater. Technol.*, 2020, **26**, e00226.
45 L. Gao, X. Li, Y. Liu, J. Fang, S. Huang, I. Spanopoulos, X. Li, Y. Wang, L. Chen, G. Yang and M. G. Kanatzidis, *ACS Appl. Mater. Interfaces*, 2020, **12**, 43885–43891.
46 W. Zhang, J. Xiong, J. Li and W. Daoud, *J. Mater. Chem. A*, 2019, **7**, 9486.
47 K. Leng, I. Abdelwahab, I. Verzhbitskiy, M. Telychko, L. Chu, W. Fu, X. Chi, N. Guo, Z. Chen, Z. Chen, C. Zhang, Q.-H. Xu, J. Lu, M. Chhowalla, G. Eda and K. P. Loh, *Nat. Mater.*, 2018, **17**, 908–914.
48 Q. Liao, J. Chen, L. Zhou, T. Wei, L. Zhang, D. Chen, F. Huang, Q. Pang and J. Z. Zhang, *J. Phys. Chem. Lett.*, 2020, **11**, 8392–8398.
49 C. Li, H. Wang, F. Wang, T. Li, M. Xu, H. Wang, Z. Wang, X. Zhan, W. Hu and L. Shen, *Light: Sci. Appl.*, 2020, **9**(1), 31.
50 W. Ke, C. Xiao, C. Wang, B. Saparov, H.-S. Duan, D. Zhao, Z. Xiao, P. Schulz, S. P. Harvey, W. Liao, W. Meng, Y. Yu, A. J. Cimaroli, C.-S. Jiang, K. Zhu, M. Al-Jassim, G. Fang, D. B. Mitzi and Y. Yan, *Adv. Mater.*, 2016, **28**, 5214–5221.
51 D. Prochowicz, M. M. Tavakoli, A. Q. Alanazi, S. Trivedi, H. Tavakoli Dastjerdi, S. M. Zakeeruddin, M. Grätzel and P. Yadav, *ACS Omega*, 2019, **4**, 16840–16846.
52 D. Wang, W. Li, W. Sun, X. Liu, G. Li, Z. Wu, J. Wu and Z. Lan, *Electrochim. Acta*, 2021, **365**, 137360.
53 H. Zhang, Z. Chen, M. Qin, Z. Ren, K. Liu, J. Huang, D. Shen, Z. Wu, Y. Zhang, J. Hao, C.-s Lee, X. Lu, Z. Zheng, W. Yu and G. Li, *Adv. Mater.*, 2021, **33**, 2008487.
54 Y. Dong, D. Lu, Z. Xu, H. Lai and Y. Liu, *Adv. Energy Mater.*, 2020, **10**, 2000694.
55 Y. Wang, X. Liu, T. Zhang, X. Wang, M. Kan, J. Shi and Y. Zhao, *Angew. Chem., Int. Ed.*, 2019, **58**, 16691–16696.
56 Y. Xu, Y. Li, Y. Lei, Q. Wang, H. Yao, X. Zhou, Q. Zhou, Z. Ci and Z. Jin, *J. Mater. Chem. C*, 2022, **10**, 1746–1753.
57 Q. Li, Y. Dong, G. Lv, T. Liu, D. Lu, N. Zheng, X. Dong, Z. Xu, Z. Xie and Y. Liu, *ACS Energy Lett.*, 2021, **6**, 2072–2080.
58 Y. Huang, L. Qiao, Y. Jiang, T. He, R. Long, F. Yang, L. Wang, X. Lei, M. Yuan and J. Chen, *Angew. Chem., Int. Ed.*, 2019, **58**, 17834–17842.
59 I. B. Obot, N. K. Ankah, A. A. Sorour, Z. M. Gasem and K. Haruna, *Sustainable Mater. Technol.*, 2017, **14**, 1–10.
60 Y. Han, H. Zhao, C. Duan, S. Yang, Z. Yang, Z. Liu and S. Liu, *Adv. Funct. Mater.*, 2020, **30**, 1909972.

